CORE
Metadata, citation and similar papers at core.ac.uk
Provided by Okayama University Scientific Achievement Repository

1 # Measurement of the Seebeck coefficient under high
2 # pressure by dual heating

3

4 Takashi Yoshino[1]*, Ran Wang[1], Hitoshi Gomi[1,2], Yoshihisa Mori[3]
5 [1]Institute for Planetary Materials, Okayama University, Misasa, Tottori 682-0193, Japan
6 [2]Earth and Life Science Institute, Tokyo Institute of Technology, Tokyo 152-8550,
7 Japan
8 [3]Department of Applied Science, Okayama University of Science, Ridai 1-1, Kita-ku,
9 Okayama 700-0005, Japan
10

11 *Corresponding author. Tel: +81-0858-43-3737; Fax: +81-0858-43-2184.
12 E-mail address: tyoshino@misasa.okayama-u.ac.jp
13

14 **Abstract**

15 This study presents a new method for measuring the Seebeck coefficient under high
16 pressure in a multi-anvil apparatus. The application of a dual-heating system enables
17 precise control of the temperature difference between both ends of the sample in a high-
18 pressure environment. Two pairs of W-Re thermocouples were employed at both ends
19 of the sample to monitor and control the temperature difference, and independent probes
20 were arranged to monitor the electronic motivate force (emf) produced by temperature
21 oscillation at a given target temperature. The temperature difference was controlled
22 within 1 K during the resistivity measurements to eliminate the influence of emf owing
23 to a sample temperature gradient. The Seebeck measurement was successfully measured
24 from room temperature to 1400 K and obtained by averaging two measured values with
25 opposite thermal gradient directions (~20 K). Thermoelectric properties were measured
26 on disk-shaped p-type Si wafers with two different carrier concentrations as a reference
27 for high Seebeck coefficients. This method is effective to determine the thermoelectric
28 power of materials under pressure.

29

30 **I. INTRODUCTION**

31 The application of pressure to thermoelectric materials produces interesting
32 property changes.[1–5] Knowledge of thermoelectric properties at high pressures is
33 therefore important for understanding not only pressure tuning of thermoelectric
34 conversion materials to improve transport properties, but also the electromagnetic
35 behavior of materials in the Earth's interior. The Seebeck coefficient describes the

36 voltage (ΔV) that develops from a given temperature difference (ΔT) in a material ($S = \Delta V/\Delta T$). The Seebeck coefficient (S) is an integral part of the heat-to-electricity conversion in thermoelectric devices, given by $zT = S^2\sigma T/\kappa$, where σ is electrical conductivity, κ is thermal conductivity, T is temperature, and z is thermoelectric figure of merit. Previous theoretical and experimental studies have suggested that particularly high zT magnitudes can be obtained in existing thermoelectric materials (e.g., PbTe, PbSe, Bi_2Te_3) at high pressure.[6–9]

43 The Seebeck coefficient is an important parameter to identify the type of electric charge carrier in a semiconductor. Although a good thermoelectric material should have only one dominant type of charge carrier type, the Earth's constituent minerals have thermoelectric contributions from both n- and p-type carriers. For example, the thermopower of olivine, the dominant mineral in the upper mantle, shows a gradual change across zero with increasing temperature, suggesting a transition from polaron dominance in conduction to magnesium vacancy dominance around 1573K.[10,11] Some thermal boundary layers are known to exist in the Earth's interior (e.g., core-mantle boundary). Large temperature gradients may affect the redox state of the Earth's deep interior by the Seebeck effect, which makes knowledge of the electrical charge polarity in constituent minerals required for understanding the redox evolution of the mantle. However, Seebeck coefficient measurements at pressures relevant to the Earth's mantle remains unreported.

56 Seebeck coefficient measurements under pressure have progressed using a Bridgman-type high-pressure apparatus at room temperature, but most recent studies

58 have involved a diamond anvil cell (DAC) .[4,5,12–14] However, DAC studies may involve
59 uncertainties in the determined properties of bulk materials owing to the small sample
60 size and unstable heating at high temperature. In contrast, thermoelectric measurements
61 in a multi-anvil apparatus allow substantially larger samples and more stable heating.
62 Several studies have therefore determined the electrical conductivity of mantle minerals
63 up to 25 GPa and 2000 K using in situ complex impedance spectroscopy in a Kawai-
64 type multi-anvil high pressure apparatus.[15] Thermal conductivity or diffusivity under
65 simultaneously high temperatures and pressures have also been measured using impulse
66 heating methods in a Kawai-type multi-anvil press.[16] However, measurements of the
67 Seebeck coefficient in a multi-anvil apparatus at high pressure remain scarce. A high-
68 pressure setup for performing the simultaneous determination of diffusivity and
69 Seebeck coefficient in a multi-anvil apparatus at room temperature was first reported by
70 Jacobsen et al.[17] Yuan et al.[18] developed a method for simultaneously measuring
71 electrical resistivity and the Seebeck coefficient at high pressure (5 GPa) and
72 temperatures up to 750 K in a cubic multi-anvil apparatus. This method uses the
73 inherent temperature gradient in samples along the axial direction of the cylindrical
74 heater, which is essential for measuring the Seebeck coefficient. The ΔT between both
75 sample ends in a high-pressure cell tends to increase with increasing average sample
76 temperature. Large uncertainties are often unavoidable at high temperature because the
77 thermoelectromotive force (emf) of the semi-conducting materials themselves is
78 typically non-linear with ΔT. Alternatively, installation of an additional heater can be
79 useful to control small ΔT between sample ends during thermoelectric power

80 measurements to allow accurate determination of the Seebeck coefficient near the target
81 temperature.
82 For this purpose, we have developed a dual-heating system for accurate ΔT control
83 between both ends of the sample in the 6-axis press installed at Institute for Planetary
84 Materials, Okayama University. Because a Kawai-type (6-8) multi-anvil press can
85 generate much higher pressures than a cubic multi-anvil press, we developed an
86 octahedron cell including dual heaters. We introduce the system specifications and
87 performance with technical and analytical protocols to determine the Seebeck
88 coefficient under high temperature and pressure conditions. This method is useful to
89 determine the thermoelectric properties of conductive materials as a function of
90 temperature at high pressure.
91
92 **II. EXPERIMENTAL METHOD**
93 **A. Principle of Seebeck coefficient measurement by dual heating**
94 Measurement of the Seebeck coefficient in materials only requires knowledge of
95 the temperature difference and voltage across two locations on the sample. The ΔT and
96 electric potential are measured from probes in direct contact with the sample ends, and
97 the Seebeck coefficient can be determined from the slope of ΔV vs. ΔT following the
98 differential method.[19] Figure 1 shows a schematic design of the Seebeck coefficient
99 measurement used in our laboratory. The probes serve as both two sets of
100 thermocouples and voltage leads from both ends of the sample. The thermocouples are
101 not involved in the emf measurement. Each thermocouple is connected to each side of a

102 disk-shaped sample through a metal electrode. Each of the dual-heating systems is

103 configured as a separate circuit from the thermopower measurement circuit. An AC

104 power supply was used for heating. Proportional-integral-differential (PID) temperature

105 control was used to generate ΔT between both ends of the sample. Each heater controls

106 the temperature at the position of the thermocouple to which it is closer located. The ΔV

107 is measured at fixed pressure and variable ΔT. The ΔV values are measured and plotted

108 to eliminate any voltage offset.[20] The Seebeck coefficient (S) is calculated from the

109 slope of the temperature difference ($\Delta T = T_1 – T_2$) and emf (ΔV) assuming linearity in S

110 for the bulk sample. The absolute Seebeck coefficient is corrected for contributions of

111 voltage from the contact wires by subtracting the Seebeck voltage produced by the

112 probe wires. In the case of the semiconductor samples with particularly larger Seebeck

113 coefficients (> 100 μV/K), however, the small emf produced by the metal leads and WC

114 anvils (~1 μV/K) can be ignored.

115

116 **B. Electrical resistivity measurement**

117 A four-wire resistance measurement design was used to measure the temperature-

118 dependence of sample electrical resistivity. In the resistivity measurement, the

119 temperature is controlled to be the same at both ends of the sample to avoid the

120 thermopower derived from the sample itself. The obtained resistance data were

121 processed to compute sample resistivity using Ohm's law, $R = \frac{V}{I}$, where R is resistance,

122 V is the voltage drop, and I is current. The sample resistivity was calculated on the basis

123 of the sample dimension $\rho = \frac{RA}{L}$ where L and A are the sample length and cross-

124 sectional area, respectively.

125

126 **C. Sample and Cell Assembly**

127 The samples used for testing are p-type Si wafers with relatively higher S than n-

128 type Si.[21] One reason for choosing Si-based materials is that the band structure of Si is

129 well known. Si-based devices are considered as an important thermoelectric materials,

130 and often applied to a refrigeration systems, such as central processing units (CPUs) or

131 field emission displays (FEDs).[22] We measured two p-type Si wafers manufactured by

132 Sinyo Co.Ltd. and Shin-Etsu Chemical Co. with low and high carrier concentrations,

133 respectively, although the exact concentration is unknown. Si wafers with a thickness of

134 0.52 mm were cored into a disk shape with 2-mm diameter using an ultrasonic drilling

135 machine.

136 A Kawai cell (6-8 type) was used for thermoelectric measurements under high

137 pressure. The cell assembly is shown in Fig. 2. A Cr_2O_3-doped MgO octahedron with an

138 edge-length of 14 mm was used as a pressure medium in second stage tungsten carbide

139 anvils with a truncation edge length of 8 mm. The outer assemblage consisted of a

140 Cr_2O_3-bearing MgO pressure medium, ZrO_2 thermal insulator, and a cylindrical MgO

141 polycrystalline sleeve. Two TiB_2-doped BN + AlN composite disk heaters with 4-mm

142 diameter and 0.3-mm thickness were set at both sides of the sample using an MgO

143 spacer. The electrodes of the sheet heater with two independent circuits were each

144 connected to the truncated WC anvil surface in the orthogonal direction. The disk-
145 shaped sample was sandwiched by Mo electrodes. One sample face was covered by a
146 Mo electrode, a $W_{97}Re_3$- $W_{75}Re_{25}$ thermocouple (0.1 mm in diameter) for temperature
147 reading, and one end of the W wire for probing the voltage difference placed at the
148 center of the sample. The junction of the other $W_{97}Re_3$- $W_{75}Re_{25}$ thermocouple and W
149 wire were set on the opposite sample face. The other end of the W wires was connected
150 to the truncation surface of the WC anvils located perpendicular to the sample surface.
151 Outside the Kawai cell, six of the eight second-stage WC anvils were used as electrodes
152 for monitoring the thermopower between both ends of the sample and dual heaters.
153 These six second-stage anvils were connected to all six first-stage anvils, each of which
154 was electrically insulated using Cu foil across the insulation plate. The two sets of
155 $W_{97}Re_3$-$W_{75}Re_{25}$ thermocouples were electrically insulated from the sheet heater by
156 MgO and exited the cell through the pyrophyllite gaskets. The wires for monitoring T_1,
157 T_2, and ΔV were connected to a Keysight 34970A data logger.
158 High-pressure and high-temperature experiments were performed in a 6-axis
159 multi-anvil apparatus. The 6-axis press has no guide blocks,[23] which allows sufficient
160 space to handle the set of lead wires and minimize short circuits during compression.
161 Each anvil of the 6-axis press is electrically insulated, which implies that even if four of
162 the six surfaces are used for dual heating, the remaining two anvils can be used as
163 electrodes for measuring emf. Reducing the numbers of probes through the gaskets is of
164 great merit in multi-anvil experiments because wire breakage frequently occurs during
165 compression.

166

167 **III. RESULTS AND DISCUSSION**

168 **A. Dual heating**

169 To ensure accurate control of ΔT between both ends of the sample, we tested the
170 dual heating performance at 5 GPa by two approaches. In case (1), the temperature on
171 one side of the sample (T_1) was held fixed while the temperature on the other side (T_2)
172 oscillated. In case (2), when T_1 deviated from the target T, T_2 was simultaneously
173 controlled in the opposite direction. The average T oscillates in the former case, whereas
174 a constant average T can be maintained in the latter case. In this oscillation mode, ΔT
175 values across the sample can be continuously adjusted from positive to negative. In both
176 cases, a maximum peak-to-peak ΔT of ±20 K was applied.

177 Examples of temperature oscillations (± 20 K) in high-temperature runs are shown
178 in Fig. 3. The temperature fluctuation was controlled within 1 K of the set value at the
179 two thermocouple junctions on both ends of the sample. For measurements at each
180 temperature, ΔT was produced around a given target temperature. The ΔT could not be
181 precisely controlled at T close to room temperature because the power required to
182 generate ΔT on both sides of the sample was too small compared with the original ΔT
183 created by a single heater. However, a control of ΔT was possible when the target T was
184 > 373 K. Accurate control of the temperature becomes impossible at T > 1473 K and the
185 heater electrode frequently broke at T > 1500 K. When both ends of the sample are held
186 at the same temperature by dual heating, the power (W) generated by each heater is
187 equivalent. In case (1) where T_1 is held fixed, W_2 increases when T_2 increases and W_1

188 correspondingly decreases. In case (2), W_1 and W_2 showed the opposite behavior. In
189 both cases, the total applied power remains nearly constant.
190

191 **B. Seebeck Coefficient measurement**

192 The Seebeck coefficient measurements of p-type Si wafers were performed over a
193 temperature range of 473–1473 K at 100-K intervals at 3 and 5 GPa. The temperature
194 dependence of the Seebeck coefficient of the bulk material was determined during both
195 the heating and the cooling cycles. The sample environment in the cell assembly usually
196 changes during heating, and electrical conductivity measurements of hydrous samples in
197 a multi-anvil press have shown different paths along heating and cooling cycles owing
198 to sample dehydration.[24] The reliability of obtained data can therefore be confirmed by
199 overlapping the Seebeck coefficient measured during both heating and cooling.

200 Our results show a linear response of voltage to changes in ΔT with the slope
201 yielding the Seebeck coefficient (Fig. 4). ΔV should ideally be zero, when $\Delta T = 0$.
202 Although a small degree of voltage offset is observed, the extent is substantially smaller
203 than ΔV produced by small changes of ΔT. The measured voltage includes not only the
204 sample but also both electrical and thermal contacts to the sample and the
205 instrumentation.

206 The Seebeck coefficient of heavily B-doped Si obtained under variable temperature
207 and constant pressure is shown in Fig. 5. The thermopower measurements were carried
208 out by maintaining a constant press load and varying the temperature. At fixed pressure
209 (5 GPa), the Seebeck coefficient decreases slightly with increasing temperature between

210 473 and 873 K, and then abruptly decreases to zero with increasing temperature above
211 973 K. Although the carrier concentration of this sample is unknown, the absolute *S*
212 value and *T*-dependence of Si are in excellent agreement with those of p-type Si with
213 carrier densities on the order of 10^{18}–10^{19} cm^{-3} measured at room pressure.[25–27] The sign
214 of *S* changes from positive to negative at ~1273 K, which is close to the melting
215 temperature of Si at 5 GPa. Previous experimental studies on the melting curve of Si I
216 (diamond structure) yield the following relation T (K) = −62.3 (1.4)P (GPa) + 1683.[28–
217 33] At 5 GPa, the melting temperature of Si is calculated to be 1372 K. The temperature
218 of the Seebeck coefficient polarity change is lower than the Si I melting temperature,
219 and is therefore not considered to be caused by melting.
220 Figure 6 shows the Seebeck coefficients of B-doped Si with low carrier
221 concentrations at 3 GPa and variable temperature up to 1273 K. The thermopowers
222 were measured at two different press loads and variable temperature up to 1000 K. The
223 Seebeck coefficient slightly decreases with increasing temperature, and then abruptly
224 decreases to negative values over the temperature range of 473–573 K. Above 573 K,
225 the Seebeck coefficient slightly decreases with increasing temperature. Electrical
226 resistivity also decreases abruptly in the same temperature range (Fig. 7). This behavior
227 is consistent with that of p-type Si with low carrier concentrations on the order of 10^{14}
228 cm^{-3} measured at room pressure,[34] which is consistent with the dopant carrier
229 concentration (4.6×10^{14} cm^{-3}) estimated from the measured electrical resistivity of this
230 sample (29 Ω·cm) at room temperature and 3 GPa.[35]
231 The results of measurements of Si with different levels of donor doping demonstrate

232 a negligible pressure effect on the thermoelectric properties of Si, and that carrier
233 concentration influences the *T*-dependent Seebeck coefficient. The temperatures at
234 which the Seebeck coefficient rapidly decreases, increases from 500 to 900 K with
235 increasing carrier concentration from 10^{14} to 10^{19} cm^{-3}. This trend agrees qualitatively
236 with results from an ab initio calculations that show the thermopower reaches a
237 maximum at an electron carrier concentration of ~10^{15} cm^{-3} at 500 K, while the
238 maximum at 900 K shifts to a higher dopant level of 10^{18} cm^{-3}.[26]
239 The Seebeck coefficient is the sum of the diffusive part and phonon drag part with
240 the former dominating thermopower in heavily doped samples and the latter dominating
241 that of pure Si.[36] However, the phonon drag effect only dominates at temperatures
242 below 300 K. For low dopant level Si, the thermopower rapidly vanishes at a distinct
243 temperature of ~500 K. The drop off of the Seebeck coefficient appears at the
244 approximate temperature range between extrinsic and intrinsic electrical resistivity.[34] At
245 this temperature, the electronic transport enters the bipolar intrinsic regime (Fig. 6). At
246 high charge carrier concentrations of about 10^{18} cm^{-3}, the intrinsic regime likely
247 becomes dominant near the melting temperature. The thermopower for Si wafers in the
248 intrinsic transport regime converges to small negative values for electrons at higher
249 temperature. Because the band gap of semiconductors generally decreases with
250 increasing temperature, the chemical potential moves toward the band edge with
251 increasing temperature in the "extrinsic" region and enters the band gap in the
252 "intrinsic" temperature region.[37] The observed drop off of the Seebeck coefficient over
253 the investigated temperature range therefore indicates that the carrier concentration

254 increases at certain temperatures, from the doping concentrations to the intrinsic values.

255

256 **IV. CONCLUSIONS**

257 We report a new technique to measure the Seebeck coefficient under high pressure

258 and high temperature in a Kawai-type mutil-anvil apparatus. We have developed a dual-

259 heating system in the 6-axis press installed at the Institute for Planetary Materials of

260 Okayama University. The dual-heating system can precisely control the temperature

261 difference between the two ends of a sample up to 1473 K and at least 5 GPa. The

262 resistivity and Seebeck coefficient of Si have been measured to evaluate the

263 effectiveness of this method. The results are in good agreement with the previous results

264 measured at ambient pressure, suggesting that the applied pressure effect does not

265 greatly affect the thermoelectric properties of Si. This approach is reliable and simple

266 with a high success rate and good reproducibility. This technique can be widely applied

267 for investigating the thermoelectrical properties of not only thermoelectric materials and

268 but also mantle and core materials in the Earth's interior.

269

270 **Acknowledgements**

271 We are grateful to D. Yamazaki, N. Tsujino, I. Ezenwa, N. Nakano for their insightful

272 comments. We also thank two anonymous reviewers for their comments. This work was

273 supported by the Ministry of Education, Culture, Sports, Science, and Technology of

274 the Japanese Government, Grant Numbers, 15H05827 and 17H01155 to T.Y and

275 17K06847 to Y. M.

276 References

277 [1]M. W. Schaefer and A. W. Webb, Rev. Sci. Instrum. 59, 2479 (1988).

278 [2] S. V. Ovsyannikov and V. V. Shchennikov, Phys. Sat. Sol. B 241(14), 3231–3234
279 (2004).

280 [3]S. V. Ovsyannikov, V. V. Shchennikov, Y. S. Ponosov, S. V. Gudina et al., J. Phys. D:
281 Appl. Phys. 37, 1151–1157 (2004).

282 [4]O. B. Tsiok, L. G. Khvostantsev, I. A. Smirnov, and A. V. Golubkov, J. Exp. Theor.
283 Phys. 100, 752 (2005).

284 [5]N. V. Morozova, S. V. Ovsyannikov, I. V. Korobeinikov, A. E. Karkin, K. Takarabe,
285 Y. Mori, S. Nakamura, and V. V. Shchennikov, J. Appl. Phys. 115, 213705 (2014).

286 [6]V. V. Shchennikov and S. V. Ovsyannikov, Solid State Commun. 126, 373 (2003).

287 [7]S. V. Ovsyannikov and V. V. Shchennikov, Appl. Phys. Lett. 90, 122103 (2007).

288 [8]B. Chen, Y. Li, and Z.-Y. Sun, J. Electron. Mater. 47, 3099 (2018).

289 [9]N.V. Morozova, I. V. Korobeinikov, S. V. Ovsyannikov, J. Appl. Phys. 125, 220901
290 (2019).

291 [10]R. N. Schock, A. Duba, T. J. Shankland, J. Geophys. Res. 94, 5829–5839 (1989).

292 [11]S. Constable, J. J. Roberts, Phys. Chem. Mineral. 24, 319–325 (1997).

293 [12]V. V. Shchennikov, S. V. Ovsyannikov, A. Y. Derevskov, V. V. Shchennikov, Jr, J.
294 Phys. Chem. Sol. 67, 2203–2209 (2006).

295 [13]S. V. Ovsyannikov, V. V. Shchennikov, G. V. Vorontsov, A. Y. Manakov et al., J.
296 Appl. Phys. 104, 053713 (2008).

297 [14]V. V. Shchennikov, S. V. Ovsyannikov, G. V. Vorontsov, and V. V. Kulbachinskii, J.
298 Phys.: Conf. Ser. 215, 012185 (2010).

299 [15]T. Yoshino, Surv. Geophys. 31, 163–206 (2010).

300 [16]M. Osako, E. Ito, A. Yoneda, Phys. Earth Planet. Inter. 143–144, 311–320 (2004).

301 [17]M. K. Jacobsen, W. Liu, and B. Li, Rev. Sci. Instrum. 83, 093903 (2012).

302 [18]B. Yuan, Q. Tao, X. Zhao, K. Cao, T. Cui, X. Wang, and P. Zhu, Rev. Sci. Instrum.
303 85, 013904 (2014).

304 [19]J. Martin, T. Tritt, and C. Uher, J. Appl. Phys. 108, 121101 (2010).

305 [20]V. Ponnambalam, S. Lindsey, N. S. Hickman, and T. M. Tritt, Rev. Sci. Instrum. 77,
306 073904 (2006).

307 [21]O. Yamashita, J. Appl. Phys. 95, 178–183 (2004).

308 [22]F. Salleh, K. Asai, A. Ishida, H. Ikeda, Appl. Phys. Exp. 2. 071203 (2009)
309 [23]E. Ito, T. Katsura, D. Yamazaki, A. Yoneda, M. Tado, T. Ochi, E. Nishibara, A.
310 Nakamura, Phys. Earth Planet. Inter., **174,** 264–269 (2009).
311 [24]T. Yoshino, T. Matsuzaki, S. Yamashita, T. Katsura, Nature 443, 973–976 (2006).
312 [25]A. Ohishi, X. Xie, Y. Miyazaki, Y. Aikebaier, H. Muta, K. Kurosaki, S. Yamanaka,
313 N. Uchida, T. Tada, Jpn. J. Appl. Phys. 54, 071301 (2015).
314 [26]N.F. Hinsche, I. Mertig, and P. Zahn, J. Phys. Condens. Matter 23, 295502 (2011).
315 [27]A. Stranz, J. Kahler, A. Waag, and E. Peiner, J. Electron. Mater. 42, 2381 (2013).
316 [28]A. Jayaraman, W. Klement, G.C. Kennedy, Phys. Rev. 130, 540 (1963).
317 [29]F. P. Bundy, J. Chem. Phys. 41, 3809 (1964).
318 [30]J. Lees, B.H.J. Williamson, Nature 208, 278 (1965).
319 [31]V. V. Brazhkin, A. G. Lyapin, S. V. Popova, R. N. Voloshin, Phys. Rev. B 51, 7549
320 (1995).
321 [32]G. A. Voronin, C. Pantea, T. W. Zerda, L. Wang, Y. Zhao, Phys. Rev. B 68, 020102
322 (2003).
323 [33]A. Kubo, Y. Wang, C. E. Runge, T. Uchida, B. Kiefer, N. Nishiyama, T. S. Duffy, J.
324 Phys. Chem. Solid. 69, 2255–2260 (2008).
325 [34]T. H. Geballe and G. W. Hull, Phys. Rev. 98, 940 (1955).
326 [35]G. Masetti, M. Severi, and S. Solmi, IEEE Transactions on Electron Devices, 30, 764
327 (1983).
328 [36]L. Weber and E. Gmelin: Appl. Phys. A 53, 136 (1991).
329 [37]M. Akasaka, T. Iida, A. Matsumoto, K. Yamanaka, Y. Takanashi, T. Imai, and N.
330 Hamada, J. Appl. Phys. 104, 013703 (2008)
331
332

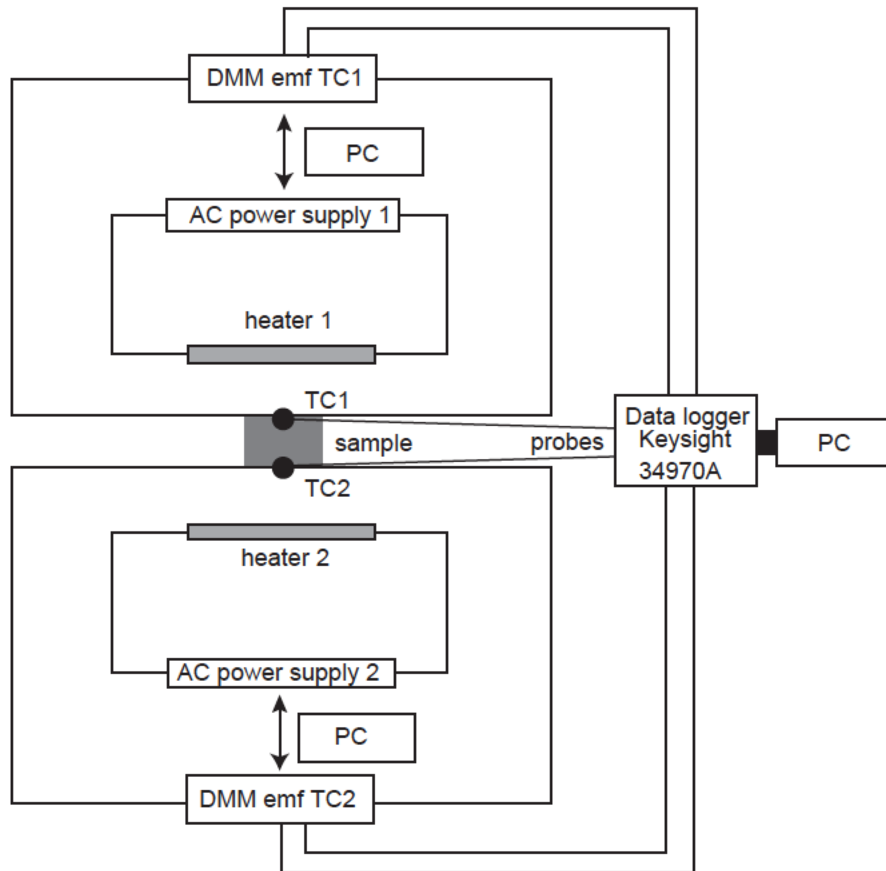

333

334 FIG. 1. Schematic drawing of the Seebeck coefficient and resistivity measurement setup

335 by dual heating in a Kawai-type multi-anvil apparatus. Temperatures at two ends of the

336 sample are monitored by two sets of thermocouples, and two resistive heaters are

337 separately computer-controlled. A data logger (Keysight 34970A) collects T_1, T_2 and ΔV

338 data as a function of time.

339

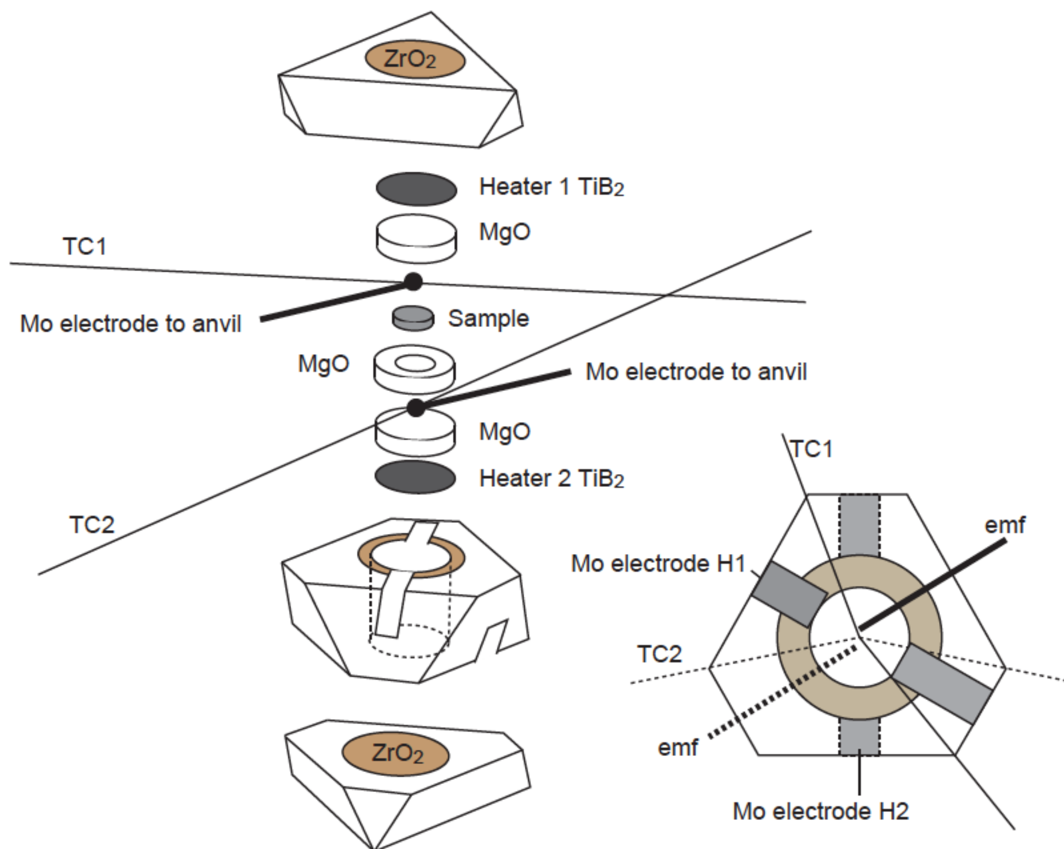

340

341 FIG. 2. Schematic illustration of the octahedron cell assembly used for the Seebeck

342 coefficient and resistivity measurements.

343

344

345

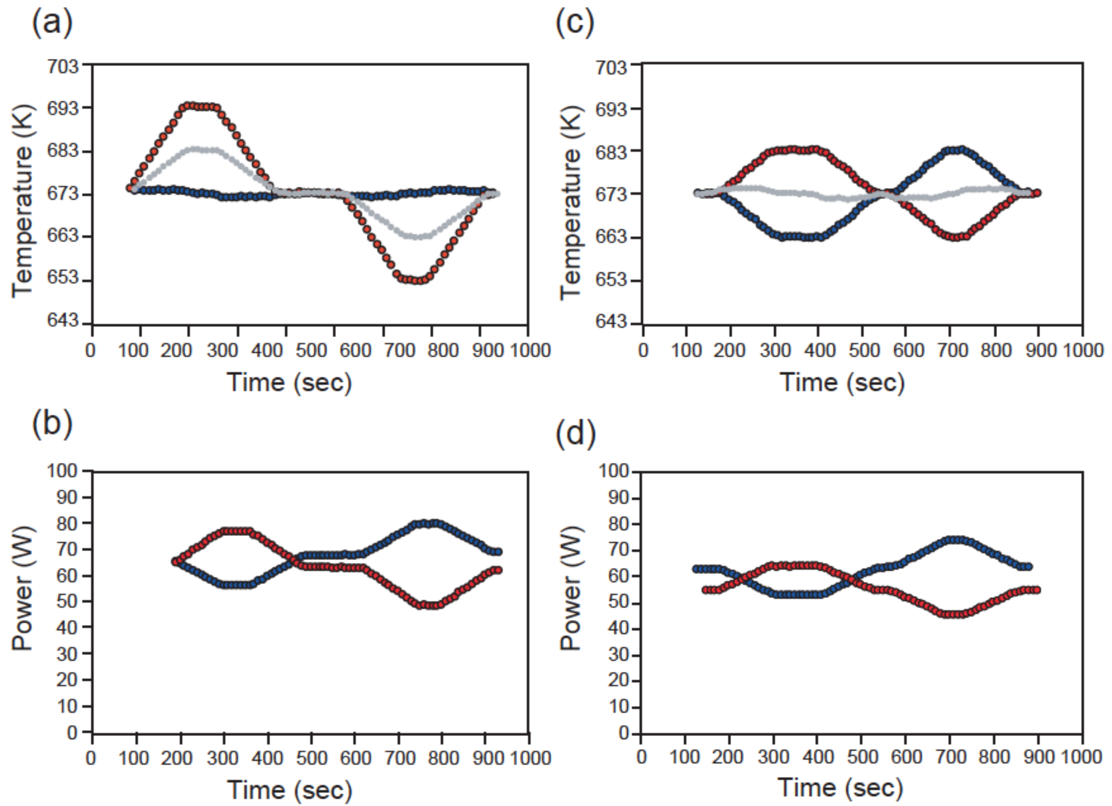

346

347 FIG. 3. Variations of temperature and heating power during the Seebeck coefficient

348 measurement at 673 K by dual heating for case 1 with the fixed T_1 and case (2) where

349 the temperatures of T_1 and T_2 oscillate in opposite directions. The top, bottom, and

350 average temperature of the sample are shown as a function of time for (a) case 1 and (c)

351 case 2. Red, blue, and gray circles denote T_1, T_2, and average temperature, respectively.

352 The applied power for heating at the top and bottom heaters is shown as a function of

353 time for (b) case 1 and (d) case 2. Red and blue circles denote applied powers W_1 and

354 W_2 for heaters 1 and 2, respectively.

355

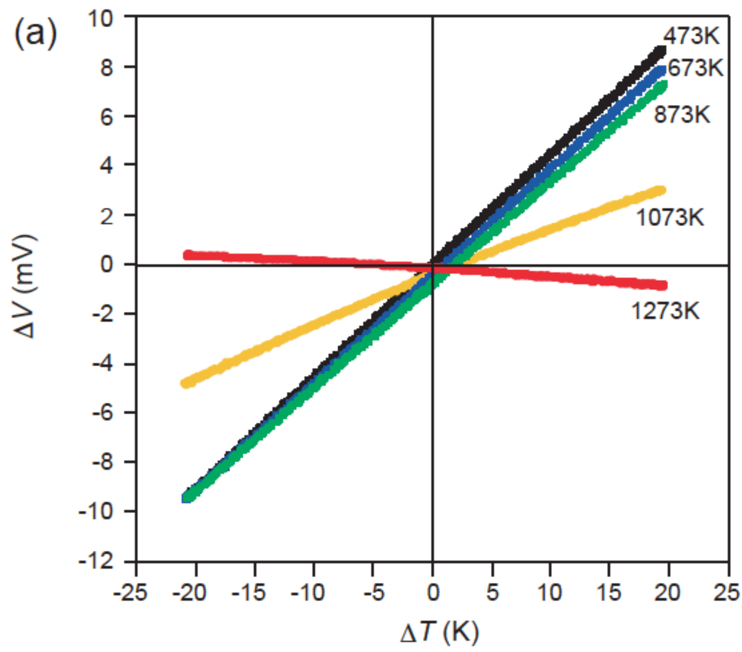

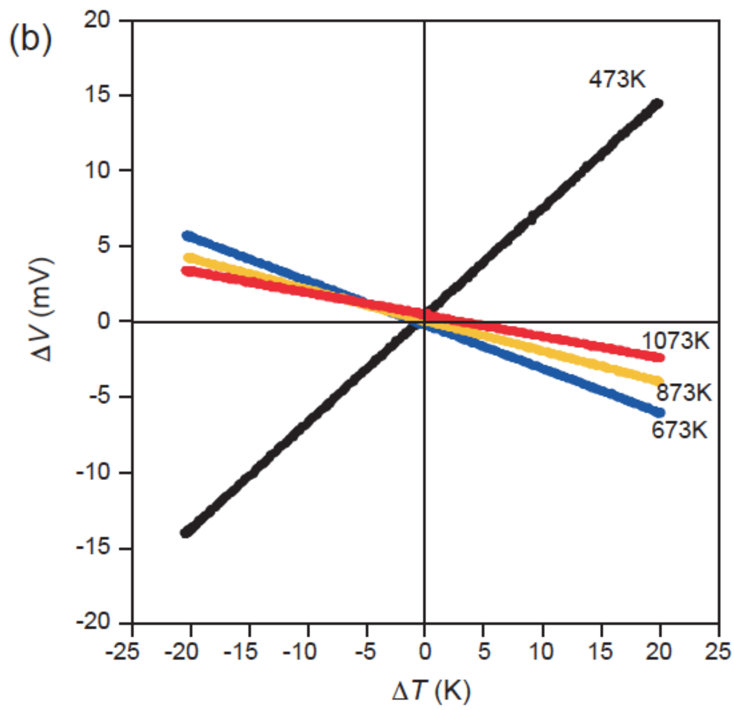

356

357 FIG. 4. Voltage response to the temperature difference (ΔT) for (a) the heavily B-doped

358 Si at 473, 673, 873, 1073, and 1273 K and (b) Si with low carrier concentration at 473,

359 673, 873, and 1073 K.

360

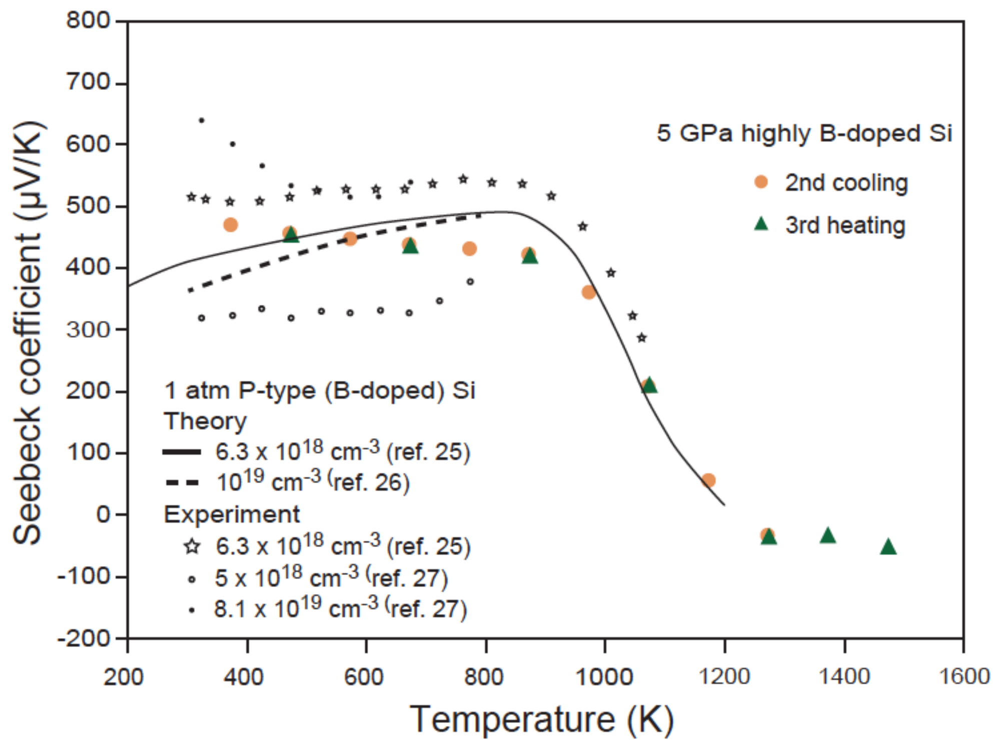

361

362 FIG 5. Temperature dependence of the Seebeck coefficient of p-type Si with high

363 carrier concentration at 5 GPa. Also shown are previously reported Seebeck coefficients

364 of Si with high carrier concentrations ($10^{18–19}$ cm^{-3}).[22–24]

365

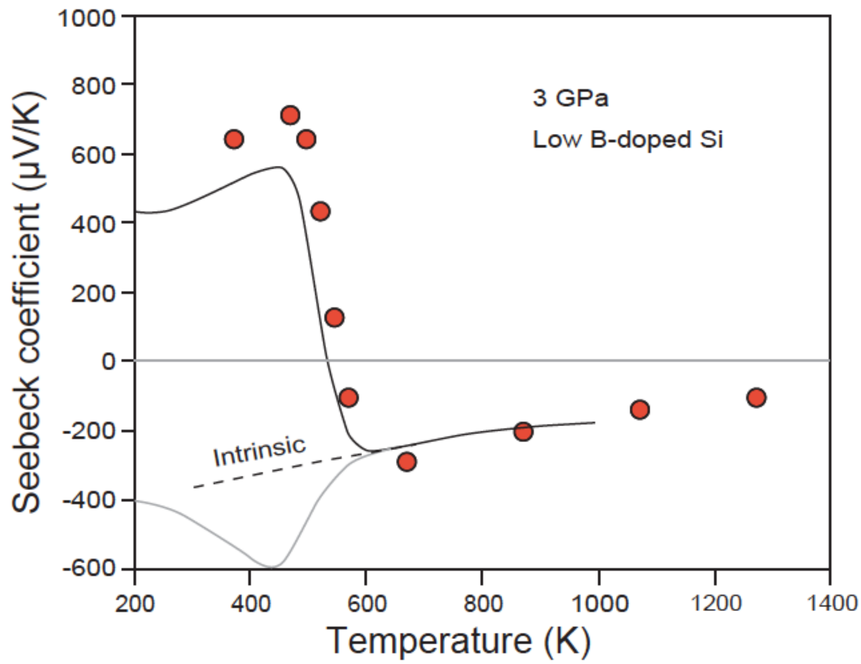

366

367 FIG. 6. Seebeck coefficient of p-type Si with low carrier concentration at 3 GPa as a

368 function of temperature. Solid and gray lines indicate calculated values[31] for p- and n-

369 type Si, respectively. The dashed line represents the calculated Seebeck coefficients for

370 the intrinsic regime[31].

371

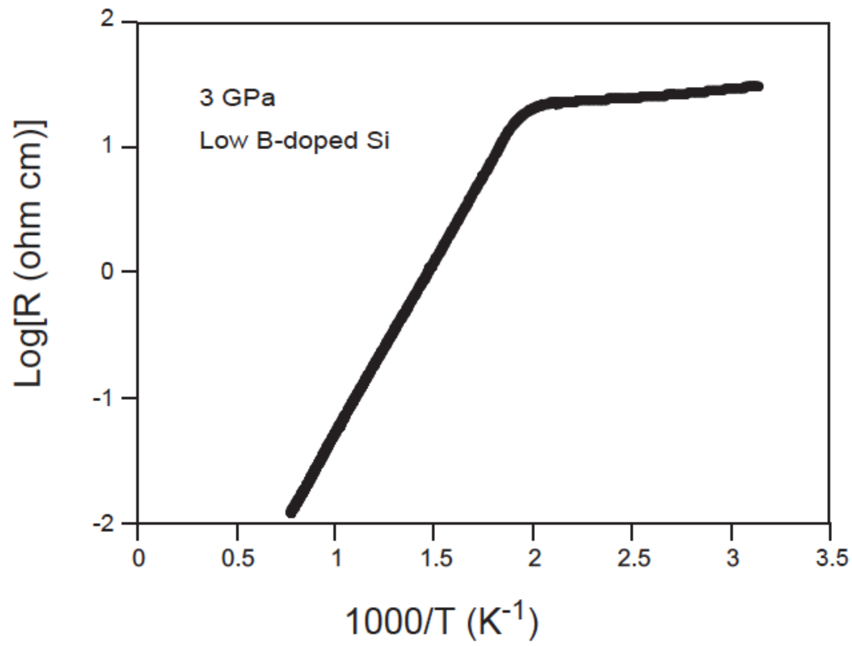

372

373 FIG. 7. Electrical resistivity of p-type Si with low carrier concentration at 3 GPa as a

374 function of reciprocal temperature.

375

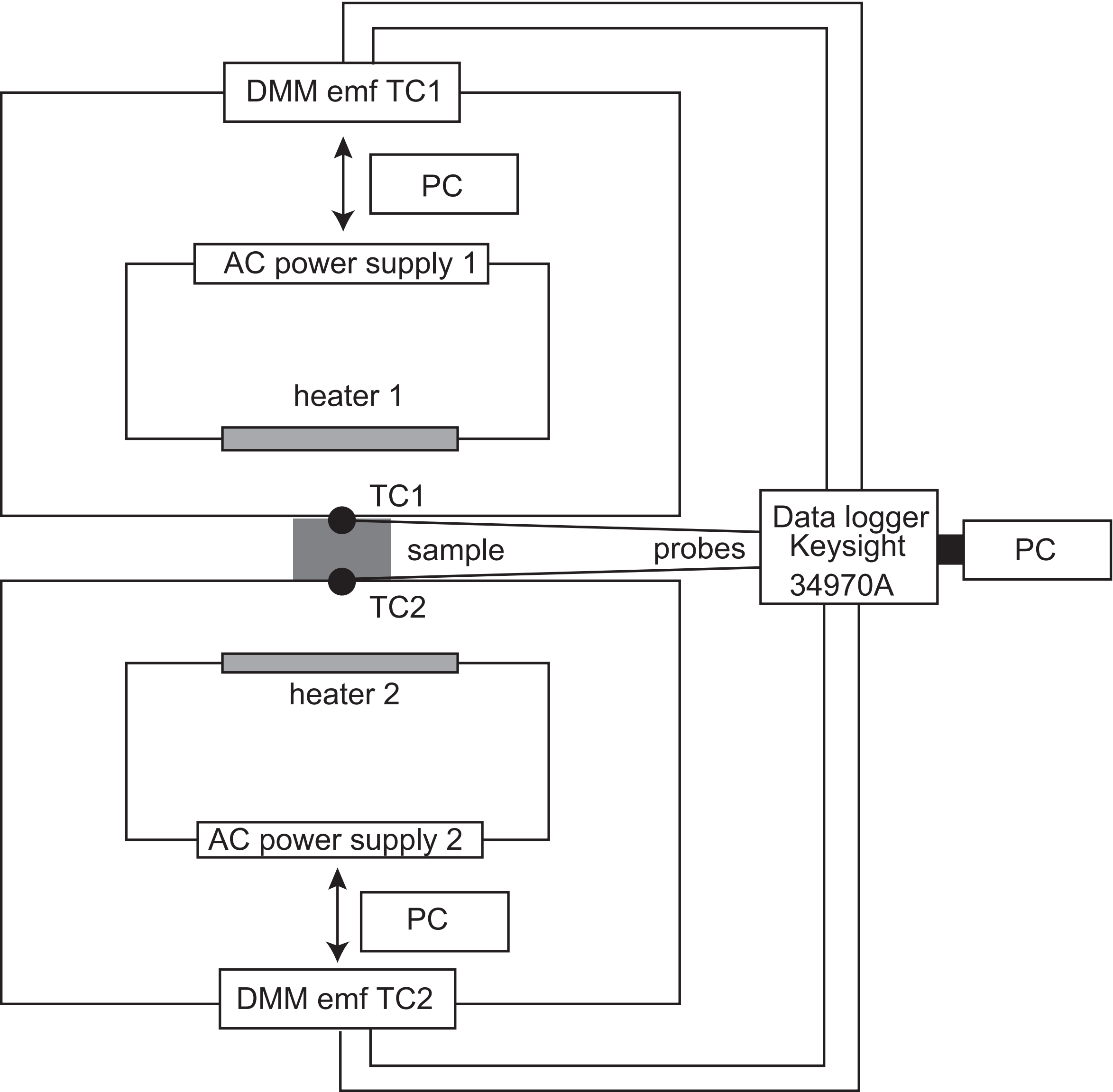

DMM emf TC1
PC
AC power supply 1
heater 1
TC1
sample
probes
Data logger
Keysight
34970A
PC
TC2
heater 2
AC power supply 2
PC
DMM emf TC2

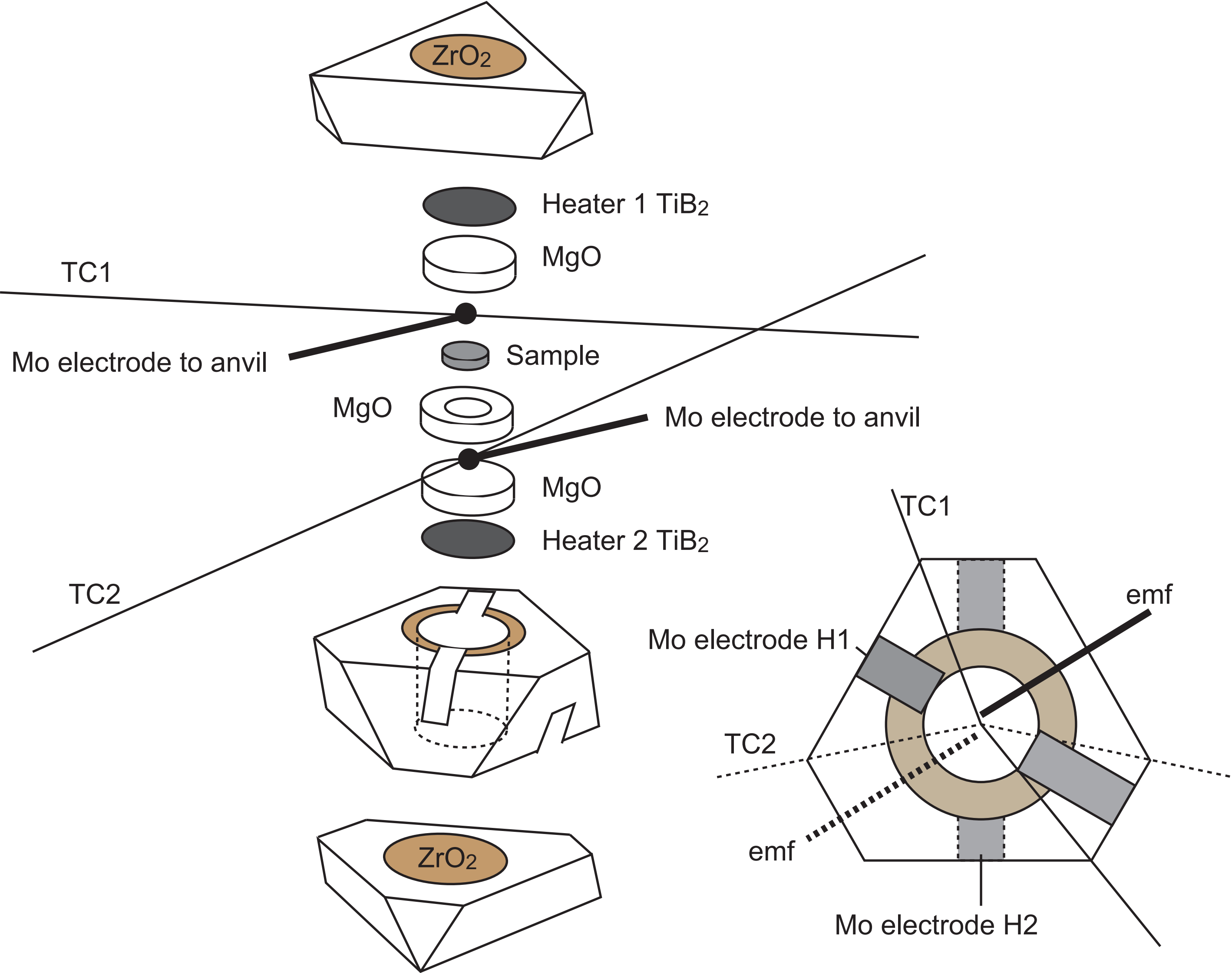

ZrO2
Heater 1 TiB2
MgO
TC1
Mo electrode to anvil
Sample
MgO
Mo electrode to anvil
MgO
Heater 2 TiB2
TC2
TC1
emf
Mo electrode H1
TC2
emf
Mo electrode H2
ZrO2

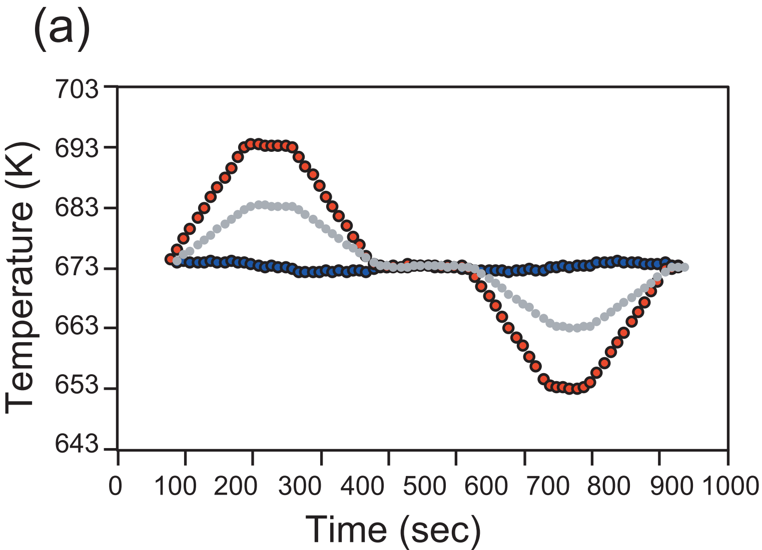
(a)
Temperature (K)
703
693
683
673
663
653
643
0
100
200
300
400
500
600
700
800
900
1000
Time (sec)
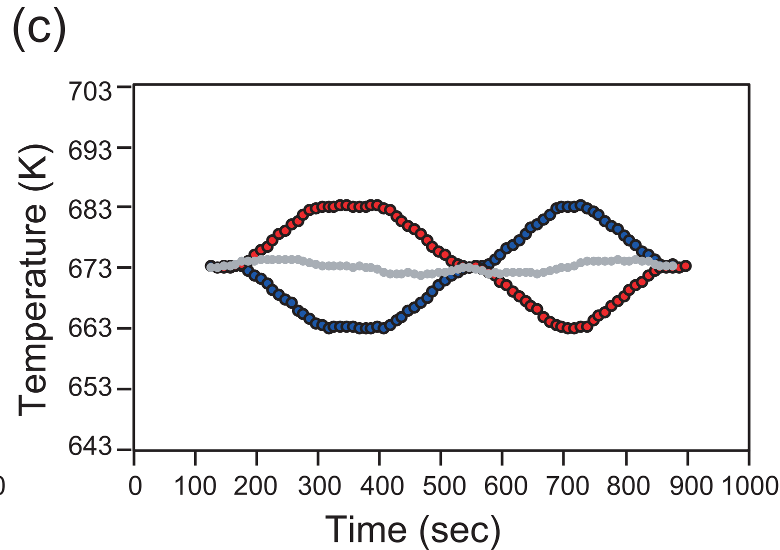
(c)
Temperature (K)
703
693
683
673
663
653
643
0
100
200
300
400
500
600
700
800
900
1000
Time (sec)
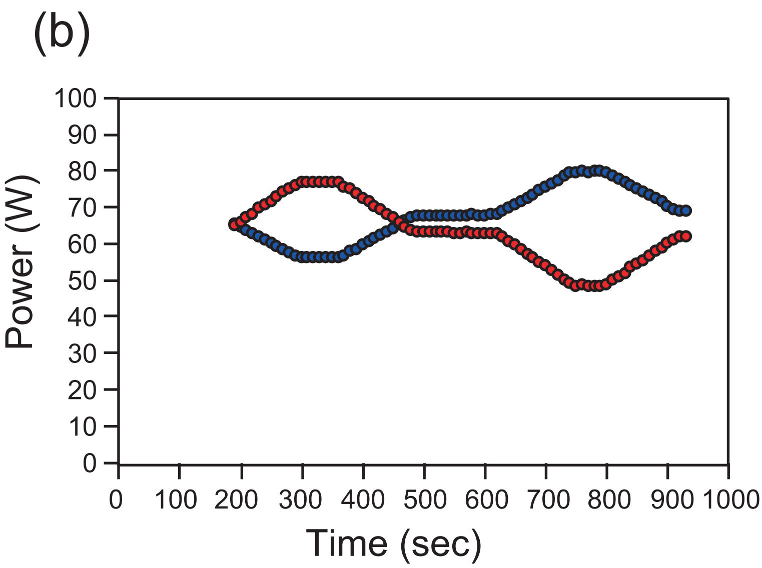
(b)
Power (W)
100
90
80
70
60
50
40
30
20
10
0
0
100
200
300
400
500
600
700
800
900
1000
Time (sec)
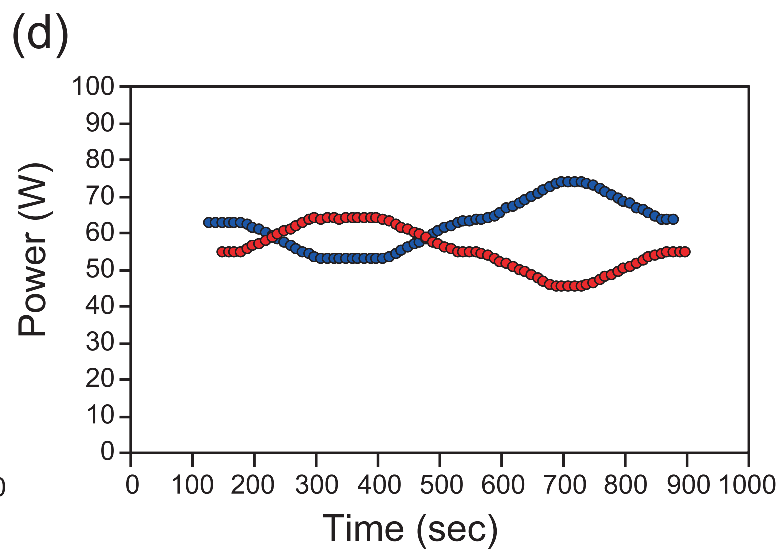
(d)
Power (W)
100
90
80
70
60
50
40
30
20
10
0
0
100
200
300
400
500
600
700
800
900
1000
Time (sec)

(a)

473K
673K
873K
1073K
1273K

ΔV (mV)

ΔT (K)

(b)

473K
1073K
873K
673K

ΔV (mV)

ΔT (K)

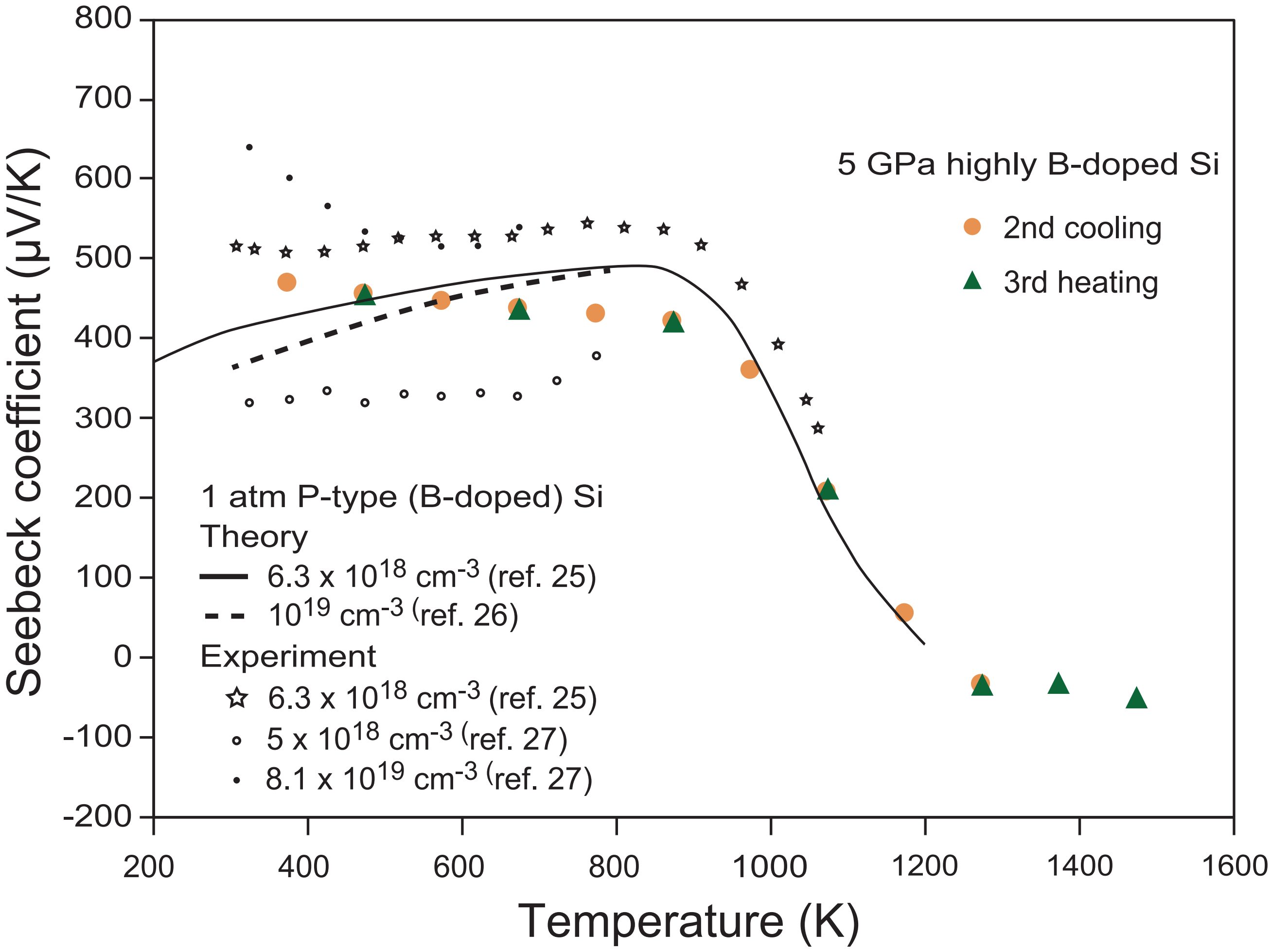

Seebeck coefficient (μV/K)
800
700
600
500
400
300
200
100
0
-100
-200
200
400
600
800
1000
1200
1400
1600
Temperature (K)
5 GPa highly B-doped Si
2nd cooling
3rd heating
1 atm P-type (B-doped) Si
Theory
6.3 x 10^18 cm^-3 (ref. 25)
10^19 cm^-3 (ref. 26)
Experiment
6.3 x 10^18 cm^-3 (ref. 25)
5 x 10^18 cm^-3 (ref. 27)
8.1 x 10^19 cm^-3 (ref. 27)

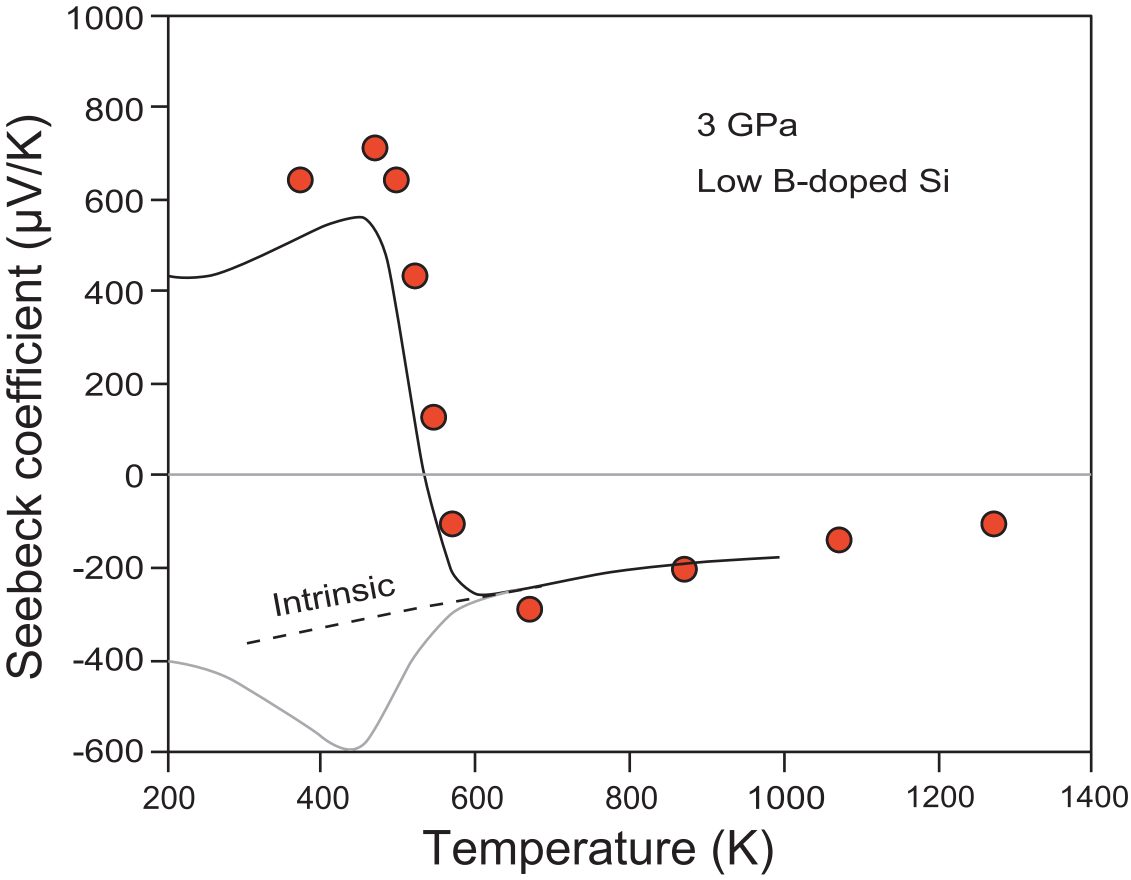
3 GPa
Low B-doped Si
Intrinsic
Seebeck coefficient (μV/K)
Temperature (K)
1000
800
600
400
200
0
-200
-400
-600
200
400
600
800
1000
1200
1400

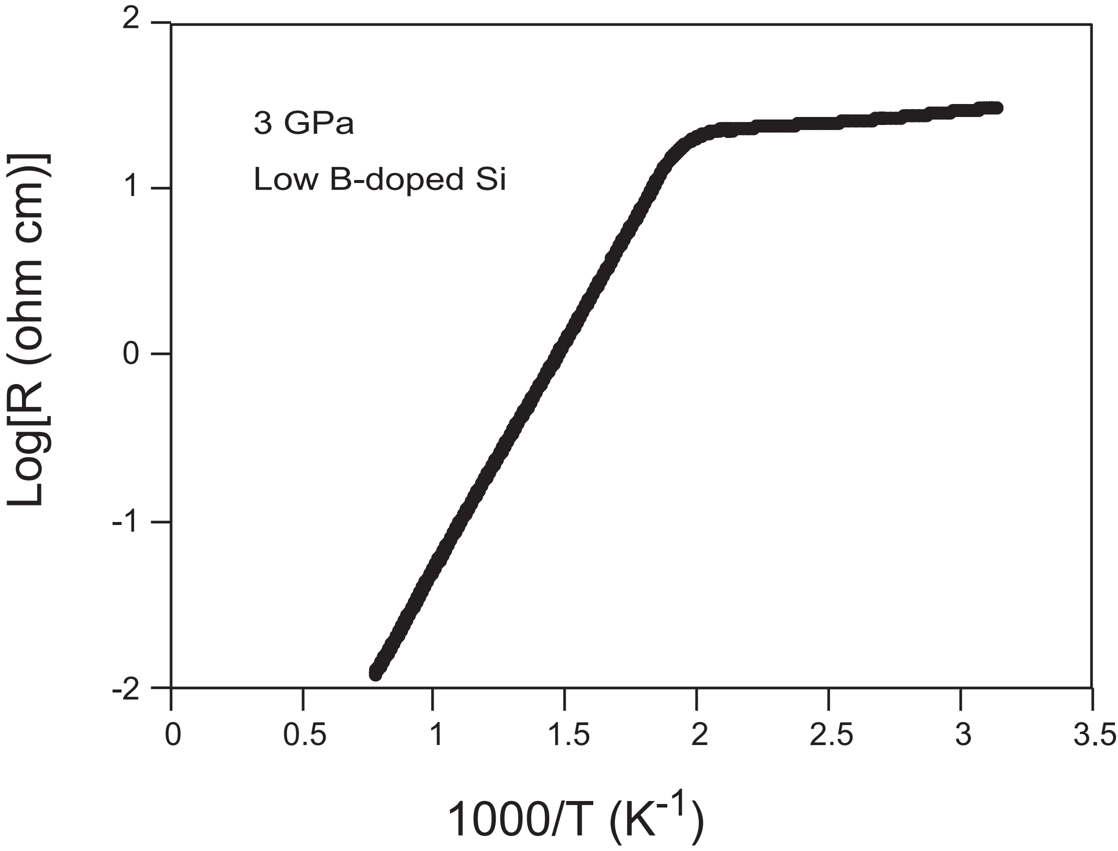
3 GPa
Low B-doped Si
Log[R (ohm cm)]
2
1
0
-1
-2
0
0.5
1
1.5
2
2.5
3
3.5
1000/T (K-1)